Atty. Dkt. No. 085802-0111

IN THE UNITED STATES PATENT AND TRADEMARK OFFICE

Applicant: Arpita I. MEHTA, *et al.*

Title: COMBINATORIAL THERAPY FOR PROTEIN SIGNALING DISEASES

Appl. No.: 10/798,799

Filing Date: 03/10/2004

Examiner: Christopher M. Gross

Art Unit: 1639

Confirmation Number: 5611

ARTIFACT SUBMISSION UNDER 37 CFR 1.91 and 1.94

Commissioner for Patents
P.O. Box 1450
Alexandria, VA 22313-1450

Sir:

Attached is a copy of the Declaration Under 37 C.F.R. § 1.132 previously filed with the U.S. Patent and Trademark Office on August 1, 2008. This Declaration includes color Appendices which were not able to be clearly scanned for IFW. This submission is in compliance with 37 C.F.R. § 1.91(a)(2) and was specifically required by Examiner Gross to address the IFW issue identified above.

Respectfully submitted,

Date August 6, 2008
FOLEY & LARDNER LLP
Customer Number: 22428
Telephone: (202) 672-5483
Facsimile: (202) 672-5399

By _____
Richard C. Peet
Attorney for Applicant
Registration No. 35,792

IN THE UNITED STATES PATENT AND TRADEMARK OFFICE

Applicant: Arpita I. MEHTA, *et al.*

Title: COMBINATORIAL THERAPY FOR PROTEIN SIGNALING DISEASES

Appl. No.: 10/798,799

Filing Date: 3/10/2004

Examiner: Christopher M. Gross

Art Unit: 1639

Confirmation Number: 5611

DECLARATION UNDER 37 C.F.R. § 1.132

Commissioner for Patents
P.O. Box 1450
Alexandria, VA 22313-1450

Sir:

1. My name is Lance A. Liotta. I am an inventor of the present application, U.S. application serial No. 10/798,799 ("the '799 application").

2. I graduated from Case Western Reserve University with an M.D. degree and a Ph.D. degree in biomedical engineering. I have worked for the National Institutes of Health for 26 years as a cancer researcher. I have published more than 600 peer-reviewed scientific articles, and received for than 50 scientific awards, including American Association Cancer Research and Public Health Service award for laser capture microdissection. I am an inventor of about 80 U.S. patents and patent applications. Presently, I am a research scientist at George Mason University and scientist at Theranostics Health, which is the exclusive licensee of the present application.

3. I performed or caused to be performed the following experiments relating to the analysis of abnormal cell signaling pathways in diseased cells.

Analysis of Protein Signaling Networks in Metastatic Ovarian Carcinoma

4. Unlike other solid epithelial tumors, ovarian cancer is spread initially by surface shedding into the peritoneal cavity followed by invasive implantation. Approximately 70% of patients with ovarian cancer present with International Federation of Gynecology and Obstetrics Stage II or IV disease, indicating that they have metastatic dissemination to the peritoneum beyond the pelvis. Accordingly, prognosis for the majority of patients with ovarian cancer is governed by the behavior of the disseminated metastatic cells and not by the primary tumor.

5. We followed the LCM and RPPA technology protocols described in the '799 application to profile a matched cohort of primary and metastatic ovarian carcinomas. A total of 15 frozen tissue samples were obtained from nine patients with a diagnosis of Stage II or IV epithelia ovarian cancer. Six patient had matched primary ovarian tissue and omental metastases obtained during cytoreductive surgery. The histological diagnoses comprised papillary serous, endometrioid and mixed carcinomas and one primary peritoneal carcinoma. Epithelial cells were microdissected from frozen tumor sections and printed on the arrays as described in the '799 application. The slides were then probed with 26 phosphospecific antibodies to proteins involved in mitogenesis including growth factor receptors, signal transducing proteins and nuclear transcription factors to profile the phosphoproteomic signal pathway circuitry (Appendix 1).

6. Analysis of the multiple different kinase substrates detected by phosphorylation-specific antibodies revealed a striking degree of patient heterogeneity in the activity of the signaling cascades within each patient. Unsupervised hierarchical clustering analysis revealed that the samples were divided into two large groups: one in which the majority of end points were activated and the other in which they were not (Appendix 2). This division was not based on primary or metastatic tissue origin or by histologic type. Interestingly the primary peritoneal carcinoma did not have a significantly different phosphoproteomic portrait than the primary ovarian tumors. The second observation was that comparison of cell signaling within the primary group itself or the metastatic group demonstrated considerable variation

in the level of signal pathway activation. There was no common pattern specific to either of the tissue microenvironments.

7. Finally, perhaps the most intriguing finding was that the metastatic signatures were dramatically changed compared with their matched primary counterparts with entirely different portraits emerging. Each patient's proteomic pattern had evolved as the tumor spread to a secondary site. In part, these results are similar to our previous work in primary ovarian cancers in that the patterns of activation in human ovarian tumors may indeed be patient-specific. The additional discovery that metastatic cell signaling is so dissimilar to the primary tumor highlights the critical need for patient-tailored therapy that is designed to specifically target the disseminated cells as it is these aberrant pathways that most likely reflect the behavior of the disease within the patient. Each of these patients is expected to respond quite differently to conventional chemotherapy despite being of similar disease stage. The acquired change in the tumor proteome may indeed be associated with drug resistance.

8. Principle component analysis identified several phosphorylated proteins that represented most of the variation between primary and metastatic tissue expression patterns. These included phosphorylated forms of c-Kit, Ask, myristoylated alanine-rich C kinase substrate, IκBα, and Ras-GRF. Most the primary and metastatic tumors could be distinguished from each other by phosphorylated c-Kit expression alone. As shown in Appendix 3, 13 of 15 tissue samples could be categorized as either primary or secondary origin. The c-Kit gene encodes a transmembrane receptor tyrosine kinase, a family of receptors that play important roles in the regulation of cellular proliferation and differentiation.

9. Our results revealed important insights into the most optimal therapeutic formula for advanced ovarian cancer. The transition from primary to secondary site correlated with activation of c-Kit. The patients therefore may specifically benefit from Gleevec therapy. In addition, the heterogeneity among patients in cell signaling requires that Gleevec must

be combined with one or more specifically selected therapeutic agents as revealed by RPPA of individual patients.

Apoptosis Pathways Reveal Prognostic Factors in Follicular Lymphoma

10. Follicular lymphoma (FL) is the second most common non-Hodgkin's lymphoma and generally is incurable. Reliable prognostic markers to differentiate patients who progress rapidly from those who survive for years with indolent disease have not been established. Most cases overexpress Bcl-2, but the pathogenesis of FL remains incompletely understood. To determine whether a proteomic approach could help overcome these obstacles, we procured lymphoid follicles from 20 cases of FL and 15 cases of benign follicular hyperplasia (FH) using laser capture microdissection. Lymphoid follicles were isolated from cases of FL and FH using laser capture microdissection (Appendix 4A) and reverse-phase protein microarrays (Appendix 4B) as described in the '799 application. The arrays were probed with antibodies to 21 proteins related to apoptosis, including phosphorylated and cleared forms. All antibodies were validated by Western blot (Appendix 4C). Arrays were scanned and dilution curves were used to quantitate relative protein expression (Appendix 4D). Test arrays showed mean intraarray and interarray coefficients of variation of 7.8% and 7.7%, respectively. Sensitivity was <50 fg/AL A panel of three antibodies [phospho-Akt(Ser^{473}), Bcl-2, and cleaved poly(ADP-ribose) polymerase] segregated most cases of FL from FH. Phospho- Akt(Ser^{473}) and Bcl-2 were significantly increased in FL ($P = 0.001$ and $P < 0.0001$, respectively). Additionally, the Bcl-2/Bak ratio completely segregated FL from FH. High ratios of Bcl-2/Bak and Bcl-2/Bax were associated with early death from disease with differences in median survival times of 7.3 years ($P = 0.0085$) and 3.8 years ($P = 0.018$), respectively. Using protein microarrays, we identified candidate proteins that may signify clinically relevant molecular events in FL. This approach showed significant changes at the posttranslational level, including Akt phosphorylation, and suggested new prognostic markers, including the Bcl-2/Bak and Bcl-2/Bax ratios.

11. *Principal component analysis segregates follicular lymphoma from follicular hyperplasia.* Principal component analysis was done to determine the panel of antibodies that could best

differentiate FL from FH. This analysis identified Bcl-2, phospho-Akt(Ser^{473}), and cleaved poly(ADP-ribose) polymerase as the strongest discriminators. Hierarchical clustering based on this panel separated the cases into two groups, one containing 13 FH cases and 3 FL cases and the other containing 17 FL cases and 2 FH cases (Appendix 5D). As expected, total Bcl-2 was significantly overexpressed in FL (expression relative to FH, 3.73 ± 2.59; P < 0.0001; Appendix 5B). Phospho-Bcl-2 expression was similar to FH (Ser^{70}, 1.32 ± 0.54; Thr^{56}, 1.11 ± 0.47). Phospho-Akt(Ser^{473}) was overexpressed in FL (2.25 ± 1.11; P = 0.001) but total Akt and phospho-Akt(Thr^{308}) were not (1.05 ± 0.38 and 1.02 ± 0.37, respectively; Appendix 5C). Phospho-Akt(Ser^{473}) expression did not correlate significantly with Bcl-2 expression (R = 0.35; P = 0.13). Cleaved poly(ADPribose) polymerase was decreased in FL (0.77 ± 0.24; Appendix 5D) although this was not significant when corrected for multiple comparisons (P = 0.023). Total poly(ADP-ribose) polymerase expression was similar in FL and FH.

12. Increased Bcl-2/Bax and Bcl-2/Bak ratios are associated with early death from follicular lymphoma. Follow-up ranged from 1.1 to 15.2 years from time of biopsy. Median overall survival was 9.3 years. Neither stage at diagnosis nor administration of chemotherapy before biopsy was significantly associated with survival. There were trends toward shorter survival times among patients with a histologic grade of 3 or a diffuse component, but these differences were not statistically significant. No individual protein showed a statistically significant association with survival.

13. Because the Bcl-2/Bax ratio has been reported to regulate apoptosis and correlate with outcome in other tumors, and Bcl-2/Bak ratios segregated FL from FH in the present study, we investigated the potential prognostic significance of these ratios in FL. Using the median Bcl-2/Bax ratio of 2.90 as a cutoff value, increased Bcl-2/Bax ratios were associated with significantly shorter survival times (median, 7.6 versus 11.4 years; P = 0.018). The mean Bcl-2/Bax ratio was 1.00 FH 0.40 in FH, 1.97 F 0.44 in FL with good outcome (survival z10 years), and 5.33 F 4.30 in FL with poor outcome (survival <10 years, excluding censored cases). Using the median Bcl-2/Bak ratio of 1.87 as a cutoff value, increased Bcl-2/Bak ratios were associated with significantly shorter survival times

(median, 4.1 versus 11.4 years; P = 0.0085). Bcl-2/Bak ratios were 0.59 F 0.17 in FH, 1.55 F 0.27 in FL with good outcome, and 2.94 F 1.73 in FL with poor outcome. Bcl-2, Bax, and Bak were not significantly associated with outcome when analyzed individually.

14. This is the first study to suggest the biological importance of the Bcl-2/Bak ratio in FL. Bcl-2/Bak ratios completely discriminated FL from FH, and patients with high ratios died significantly sooner than patients with low ratios. Bak is a conserved homologue in the Bcl-2 protein family that acts at the mitochondrial membrane to facilitate release of cytochrome c, triggering caspase activation and apoptosis. Bcl-2 inhibits the proapoptotic effects of Bak by preventing Bak oligomerization. Bak expression has been reported to be low in FL, and the cell types producing Bak in FL have not been previously reported. We showed that Bak is expressed in the neoplastic B cells of FL as well as in intermixed reactive T cells. Because T-cell density did not correlate with overall Bak expression, the prognostic significance of the Bcl-2/Bak ratio likely relates to coexpression of Bcl-2 and Bak in malignant B cells.

15. In summary, this study shows the potential of protein microarrays to identify clinically relevant molecular events in patients with FL. These events include posttranslational modifications, such as activation of Akt by phosphorylation, which are critical in apoptotic regulation. These results also suggest that Bcl-2/Bak and Bcl-2/Bax ratios are important prognostic indicators in patients with FL. Because proteins are the direct functional effectors of apoptotic decision-making in the cell, proteins that have biological importance in FL also merit investigation as potential therapeutic targets. Strategies include inhibiting Bcl-2 function or expression, enhancing activity of Bak and Bax, and disrupting Akt signaling.

Akt/Mammalian Target of Rapamycin Activation is Negatively Associated with Childhood Rhabdomyosarcoma Survival

16. We applied the reverse phase array phosphoprotein pathway mapping as described in the '799 application to evaluate whether prosurvival pathways, including Akt/mammalian target of rapamycin (mTOR), are differentially activated for rhabdomyosarcoma tumors

associated with a poor versus favorable outcome. We also tested the effect of treatment on the pathway we found to be activated in a xenograft model of human rhabdomyosarcoma. This study shows the importance of phosphoprotein cell signaling events and how they may constitute a new and functionally relevant analyte for deriving therapeutic insights for rhabdomyosarcoma.

17. *Exploratory data analysis of rhabdomyosarcoma tumor set 1A.* Enrichment of tumor cells by laser capture microdissection was done before analysis to ensure that the cells for analysis came from within the cancer cell population, without contamination by noncancer cells. For study set 1A (n = 33), 15 specific signaling proteins were initially chosen for reverse phase protein microarray analysis because they constituted a broad survey of multiple prosurvival related events related to the Akt/mTOR pathways that have been shown to play a role in rhabdomyosarcoma. Unsupervised hierarchical clustering analysis of the 15 protein end points revealed two major classes of tumors: one cluster with Akt/mTOR activation/phosphorylation and the other with a comparatively low level of signaling. After clinical outcome data was obtained from the Children's Oncology Group (COG), these two clusters were compared by Fisher's exact test based on patient characteristics of age, sex, primary site, histology, invasion, and lymph node involvement. Although none of the characteristics reached $P < 0.05$ statistical significance, patients with parameningeal head and neck primary site tumors comprised 62% of cluster 1, whereas cluster 2 had 27% of patients with parameningeal primary site tumors (Fisher's exact test, $P = 0.06$). Additionally, cluster 2 contained 73% alveolar tumors, whereas cluster 1 had 62% embryonal tumors (Fisher's exact test, $P = 0.06$). Typically, patients with embryonal rhabdomyosarcoma tumors from orbital or nonparameningeal sites have the best prognosis. These two clusters were not statistically different for commonly accepted prognostic/clinical factors associated with rhabdomyosarcoma.

18. We proceeded to correlate the protein analyte values with disease-free and overall survival clinical outcome data provided by the COG for study set 1A. A clear partitioning of the tumors emerged after clinical outcome data was obtained from the COG. A decision tree analysis of three proteins—4EBP1, phosphorylated 4EBP1 Thr37/46, and eIF4E—all

components of the Akt/mTOR pathway, partitioned patients who were in continuous complete remission from those who recurred and died after being treated with standard therapy. Among these end points, 4EBP1 and 4EBP1 $Thr^{37/46}$ individually were found to be significantly correlated with survival by Wilcoxon one-way analysis, 4EBP1 ($P < 0.0064$) and 4EBP1 $Thr^{37/46}$ ($P < 0.0135$). A log rank univariate survival analysis (Kaplan-Meier) supported the association of 4EBP1 with outcome in overall and recurrence-free survival in study set 1A (overall survival $P = 0.0177$, recurrence-free survival $P = 0.0370$).

19. For recurrence-free survival in study set 1A, 4EBP1 level ($P2 = 0.0074$; hazard ratio, 7.44; 95% confidence interval, 1.71–32.36) emerged as significant prognostic factor. Thus, for study set 1A, individual components within the Akt/mTOR pathway seemed to correlate with survival.

20. *Disease-free and overall survival in rhabdomyosarcoma patients is associated with phosphorylated components of the Akt and mTOR pathways.* Based on the findings of study set 1A, an independent set of samples (set 1B) were obtained from COG ($n = 26$) for analysis of an expanded set of proteins associated with the Akt/mTOR pathway. Univariate log-rank analysis of the two heterogeneous sample sets (set 1A and 1B) revealed no significant difference in overall or recurrence-free survival by sample set (overall survival $P = 0.2111$, recurrence-free survival $P = 0.5824$) or histology (overall survival $P = 0.4103$, recurrence-free survival $P = 0.4312$). We analyzed set 1B by laser capture microdissection and reverse phase protein microarray as in set 1A. We expanded the number of end points to 27 to include additional signaling proteins upstream and downstream of Akt and mTOR for an independent evaluation of pathway activation.

21. Following unblinding of the data, the results for study set 1B showed a significant association of disease-free and overall survival with phosphorylated components of the Akt-mTOR pathway. High levels of Akt Ser^{473}, 4EBP1 $Thr^{37/46}$, eIF4G Ser^{1108}, and p70S6 Thr^{389} were all significantly associated with poor overall and poor disease-free survival: Akt Ser^{473} (overall survival $P < 0.001$, recurrence-free survival $P < 0.0009$), 4EBP1 $Thr^{37/46}$ (overall survival $P < 0.0110$, recurrence-free survival $P < 0.0106$), eIF4G Ser^{1108} (overall

survival $P < 0.0017$, recurrence-free survival $P < 0.0072$), and p70S6 Thr^{389} (overall survival $P < 0.0085$, recurrence-free survival $P < 0.0296$). Each of the 27 components was also evaluated individually for statistical correlation with survivor versus nonsurvivor status. Six end points—again, all components of the Akt/ mTOR network (4EBP1 Thr^{37}, Akt Ser^{473}, eIF4G Ser^{1108}, p70S6 Thr^{389}, Bak, and GSK3a/h $Tyr^{279/216}$)—correlated independently with survival [Wilcoxon one-way analysis 4EBP1 Thr37/46 ($P < 0.0348$), GSK3a/h $Tyr^{279/216}$ ($P < 0.0348$), eIF4G Ser^{1108} ($P < 0.0196$), Akt Ser^{473} ($P < 0.0227$), Bak ($P < 0.0321$), and p70S6 Thr^{389} ($P < 0.0373$)].

22. *IRS-1/Akt/mTOR feedback loop is dysregulated in nonsurvivor cohort.* Although tyrosine phosphorylated insulin receptor substrate-1 (IRS-1) activates Akt/mTOR signaling through phosphatidylinositol 3-kinase (PI3K), serine phosphorylation of IRS-1 at $serine^{612}$ by mTOR and p70S6 down-regulates IRS-1 tyrosine activation (19–21). Thus, IRS-1 is subject to negative feedback regulation in response to Akt/mTOR activation (Appendix 6A). We examined levels of phosphorylated members of the IRS-1/Akt/mTOR feedback loop by reverse phase protein microarray for the tumors in study set 1B (n = 26). Although levels of IRS-1 Ser^{612} were no different between the survivors and nonsurvivors, phosphorylation of IRS-1 Ser^{612} correlated strongly with phosphorylation of mTOR at Ser^{2448} in the survivor cohort (Spearman's Rho nonparametric $P < 0.0027$), suggesting a linkage between these two signaling events (Appendix 6B). By contrast, the phosphorylation of these same two signaling proteins was not correlated in the nonsurvivor cohort (Spearman's Rho nonparametric $P = 0.7358$; Appendix 6B-6C). This lack of correlation with IRS-1 Ser^{612} phosphorylation also prevailed for the mTOR downstream components eIF4E Ser^{209} (survivor $P = 0.0006$, nonsurvivor $P = 0.102$) and p70S6 Thr^{389} (survivor $P = 0.00004$, nonsurvivor $P = 0.1827$; Appendix 6B and 6D). Thus, the interrelationship between IRS-1 activity and the mTOR pathway proteins may be altered in the tumors of patients, which subsequently are found to have poor survival after chemotherapy compared with the tumors of patients who have long-term survival (Appendix 6A-6D).

23. *Interrogation of the phosphorylated versus nonphosphorylated state of proteins.* Phosphorylation is an important posttranslational modification that has potential significance as a readout for the activation state of pathways and kinase inhibitor targets. To further investigate potential significant cell signaling proteins within the IRS-1/Akt/mTOR pathway, we extended our analysis to include the following additional end points: BAD, eIF4G, IRS-1, IRS-2, IGFR-h, and S6 $Ser^{240/244}$. We conducted Wilcoxon one-way analysis and Kaplan-Meier survival analysis for the phosphorylated protein, the total protein form, and the ratio of the phosphorylated to total forms of key protein end points (Appendix 6B). The results clearly show that the specific phosphorylated forms of the protein end points within the Akt/mTOR and associated pathways are independently associated with survival ($P < 0.05$) compared with the non-phosphorylated total form of the analyte protein (4EBP1 Thr37/46 $P < 0.035$, p70S6 Thr^{389} $P < 0.037$, Akt Ser^{473} $P < 0.023$, eIF4G Ser^{1108} $P < 0.02$). This is an important distinction because it is likely that the population of the total protein in a signal pathway node is in excess compared with the phosphorylated form. The phosphorylated form, actively engaged in signaling, constitutes a subpopulation of the total protein. Thus, the phosphorylated form constitutes a variable that is independently correlated with survival compared with the total protein (Appendix 6).

24. *Suppression of the mTOR pathway in a mouse xenograft model reduces tumor growth.* To validate the functional significance of our IRS-1/Akt/mTOR network analysis, we used rapamycin analogues, which are well-characterized inhibitors of the mTOR protein kinase pathway, using a mouse xenograft treatment model. Either RD embryonal cells or Rh30 alveolar cells were injected orthotopically into the hind leg of beige SCID mice. These two different cell lines were used to determine the effects of mTOR inhibition in different histologic tumor categories. The rapamycin analogue CCI-779 (Wyeth, Madison, NJ) dosage was 20 mg/kg, which corresponds to dosages currently administered to humans in phase I and II clinical trials. Administration of CCI-779 at doses that were verified to suppress the phosphorylation of mTOR downstream targets profoundly reduced the growth of rhabdomyosarcoma xenografts as measured in the beige SCID murine model (Rh30 xenograft group $P = 0.0002$; RD xenograft group $P = 0.00008$, $n = 8$ for both groups).

Suppression of the mTOR pathway was monitored by measuring the phosphorylation of 4EBP1 and S6 ribosomal protein, which are well-established downstream targets of mTOR. CCI-779 inhibited the phosphorylation of these downstream targets commensurate with a blockade in mTOR signaling in both the Rh30 alveolar– and RD embryonal xenograft–derived tumors. In addition, there was a slight but definite increase in phosphorylated Akt at Ser^{473} in both the RD and Rh30 xenograft tumors over the course of treatment with CCI-779.

25. In summary, protein pathway analysis of microdissected human rhabdomyosarcoma clinical specimens, procured before treatment, revealed a strong association between activation (phosphorylation) of multiple interconnected Akt/mTOR pathway components and a poor disease-free or overall survival in this initial, exploratory analysis. This observation was found to be consistent between two independently analyzed clinical study sets. Moreover, the functional significance of IRS-1/Akt/mTOR pathway activation in rhabdomyosarcoma was verified using the specific targeted inhibitor CCI-779 to suppress tumor growth in a beige SCID rhabdomyosarcoma xenograft model. These data provide impetus for testing rapamycin analogues in this tumor type as a potential way to modulate poor prognosis patients into more durable outcomes. Based on the interrelationship of the Akt/mTOR pathway and the IGF-IRS pathway (Appendix 6), future combination therapy strategies should be aimed at blocking both upstream IRS-1–mediated signaling factor activation, as well as downstream mTOR signaling, as a means of augmenting standard cytotoxic rhabdomyosarcoma therapy.

Analysis of Obesity-related Nonalcoholic Fatty Liver Disease Using Reverse Phase Protein Microarrays

26. Cell signaling pathway derangements are not unique to cancers, but are found in a variety of disease conditions. We followed the LCM and RPPA technology protocols described in the '799 application to profile cell signaling pathways in nonalcoholic fatty liver disease (NAFLD).

27. We employed RPPA technology to profile signaling events in human adipose tissue from patients with NAFLD and a matched group of obese controls. The study was designed to test the hypothesis that white adipose tissue (WAT) is a bioactive organ that influences the path physiology of NAFLD. Furthermore, we correlate changes in the specific signaling pathways active in adipose tissue from patients with different subtypes of NAFLD as a means of uncovering new biomarkers and therapeutic targets for disease mitigation.

28. *Demographic and Clinical Data.* The patient study set included 99 patients, 70 of whom had NAFLD and 29 were designated as Obese Controls because their liver biopsies did not show any significant pathological changes.

29. *Analysis of Human Adipose Tissue Phospoproteome.* Broad patient-specific heterogeneity of the active signaling events is revealed by unsupervised Bayesian clustering analysis of cellular signaling using phospho-specific endpoints (Appendix 7). Cell signaling pathways fell into expected groupings corresponding to the time course of the changes in the activity the kinases and the levels of their phosphorylated substrates. Unsupervised Bayesian approaches allow separate assessment of the kinase phosphorylation levels and its cognate substrate (*e.g.*, mitogen-activated protein kinasekinase [MEK] and extracellular regulated kinase [ERK]). Even without an *a priori* training, many of the components of the MEK-ERK kinase pathway family were grouped in the same cluster, indicating that we were able to recapitulate active networks in lysed adipose cells. The inability of an unsupervised approach to segregate NAFLD phenotypes is not surprising, and probably results from the broad signaling differences between different NAFLD subtypes and the fact that many physiological links between adipose and liver tissues are relatively weak compared with changes within the liver itself. To evaluate the potential for specific signaling pathways to provide for correlative outcomes, we took a more focused approach—studying and comparing the progressive form of NAFLD (NASH) with its relatively benign forms (SS and NSI) and evaluating each phosphorylation event as an independent variable.

30. *Molecular Network Comparison of NASH Versus Non-NASH.* To evaluate differences in molecular networks between patients with NASH and patients with the non-progressive

form of NAFLD(Non-NASH), and to understand the influence of nonspecific inflammation on any subsequent analysis, we studied each phospho-specific and signaling endpoint for significance of discrimination between NASH and SS, or between NASH and NSI. Histographical analysis revealed that phosphorylation of a member of the AKT/mTOR pathway, the forkhead transcription factor (FKHR), is elevated ($P < 0.001$) in the adipose tissue of patients with SS compared with those with NASH. Note that when all 99 morbidly obese patients were analyzed, amounts of the FKHR phosphorylated at S256 residue significantly correlated with AST/ALTratio (R=0.2706, $P < 0.015$). When the analysis is expanded to include patients with SS and NSI, decision tree partition analysis, which looks for linked principal distinguishing components, also identified the FKHR protein as an important classifier. Additionally, decision tree partitioning analysis pinpoints other members of the insulin and theAKT/mTOR pathways as being differentially phosphorylated in patients with non-progressive form of NAFLD and those with NASH.

31. It is significant and striking that although each of these endpoints was independently analyzed as an individual component of the pathway, whole pathways were highlighted, indicating broad, pathway-wide differences between NASH and non-progressive forms of NAFLD. The results indicate elevated phosphorylation of the insulin pathway in adipose tissue of patients with nonprogressive forms of NAFLD (Non-NASH) compared with NASH, except for focal adhesion kinase, for which phosphorylation appears to be relatively higher in NASH. A comparison of SS to NSI revealed additional components of the AKT/mTOR pathway, GSK3 and E1F4G, and insulin signaling pathway, SHC and PKC delta. This signal pathway profiling of omental adipose specimens from patients with NAFLD appears to differentiate patients with NASH from those with the non-progressive forms of NAFLD (SS and NSI). Analysis of many disparate signaling pathways specifically highlighted the insulin signaling network as significantly affected in fatty liver disease pathogenesis.

32. *Molecular Network Comparison of Patients with NAFLD Versus Obese Controls.* We next analyzed phospho-signaling portraits in patients with NAFLD compared with obese

controls without NAFLD to further understand pathway changes in adipose tissue, the relationship of these changes with liver pathology, and the specificity of the insulin pathway changes we observed in progressive NAFLD versus non-progressive NAFLD. Principal component analysis was also an effective tool for identifying key components of discrimination, with most obese controls segregated from subjects with NAFLD. However, although some components of the insulin pathway were part of the overall discrimination, a substantial component of the signaling differences corresponded to other pathways such as eNOS and cAbl. Amounts of cleaved caspase 9 and pp90RSK S380 were positively correlated ($R=0.5444$, $P < 3.44e\text{-}^{08}$) and were increased in patients with NASH and in those with NSI compared with the obese controls or those with SS ($P < 0.05$). The results indicate that the derangements in adipose tissue inpatients with NASH versus non-progressive form of NAFLD are fairly specific, and that other signaling changes occur in the adipose tissue of NAFLD patients compared with the obese controls.

33. This study uses a novel approach to elucidate the pathogenesis of NAFLD. Earlier studies of NAFLD have focused on histological or molecular analysis of the liver tissue. We used a systemic assessment of the influences of WAT on liver pathology to reveal new insights into the biological mechanisms of NAFLD and new therapeutic targets for treatment. We chose to focus this initial study on the global analysis of phosphorylation-driven cellular signaling within the WAT itself. We hypothosized that disease-related changes in intracellular signaling in WAT could become manifest through alterations in the autocrine and paracrine feedback loops between WAT and the liver.

34. These data strongly connect WAT to the pathogenesis of the NAFLD and NASH. In fact, patients with biopsy proven NASH displayed significant alterations in the pathways related to insulin resistance (IR) compared with obese controls and patients with SS or NSI. Given the known role of WAT in the development of IR, and the importance of IR in the initial steps of fat deposition within the hepatic parenchyma (the so-called "first hit"), these findings are not surprising. Interestingly, phosphorylation of the components of the insulin pathway was more pronounced in the adipose tissue of SS patients than in patients with NASH. A decrease in insulin signaling via the insulin receptor substrate-

1/phosphatidylinositol 3-kinase pathway should result in further reduction of glucose uptake and utilization in the livers of patients with NASH. Also, the levels of inactive, unphosphorylated insulin receptor substrate 1 were greater in the adipose tissue of patients with NASH than those with SS, perhaps because of compensatory regulation of total receptor up regulation in patients with a potentially progressive form of liver disease. Our initial observations suggest that the action of insulin in the adipose tissue of patients with non-progressive NAFLD is mediated mostly through CREB/focal adhesion kinase control of glucose metabolism, the PKC lipolysis pathway and the AKT/mTOR pro-survival/apoptosis axis. In addition to supporting the role of IR in the pathogenesis of NASH, these findings provide important potential targets for future therapeutic interventions. We also demonstrate a novel approach to the discovery of new tissue biomarkers that accurately distinguish NASH from the other subtypes of NAFLD.

35. This study provided a comprehensive analysis of cell signaling in human adipocytes obtained directly from clinical specimens. We used RPA along with a new pressure cycling technology for fat tissue solubilization to generate phosphoproteomic "portraits" of ongoing signaling in human fat specimens to study a cohort of patients with biopsy-proven NAFLD. Our data suggest that RPA technology is effective for analyzing WAT as a clinical input specimen for any relevant study.

36. The choice of WAT for this analysis made intuitive sense because it is a biologically active organ that secretes several important cytokines [*e.g.*, IL-6, tumor necrosis factor alpha (TNF-α)] and adipokines (*e.g.*, adiponectin, resistin, leptin) affecting the liver through portal or systemic circulation. In fact, growing evidence indicates that NASH is a consequence of disturbances in the signaling pathways originating from cytokines and adipokines, which can directly or indirectly (through IR) influence its pathogenesis or progression. Unfortunately, molecular pathways linking adipokines with their nuclear and cytoplasmic targets are largely unknown, so the profiling of these networks awaits the characterizations of corresponding pathways. This study is a step in that direction, because many phosphorylation events differentiating progressive and non-progressive forms of NAFLD also affect adipokine production and signaling. For example, earlier work shows

that the propagation of the insulin signal reduces the expression of adiponectin receptors AdipoR1/R2 via the phosphoinositide 3-kinase/Foxo1-dependent pathway. Increased phosphorylation of the transcription factor FKHR/FOXO1 leads to its exclusion form the nucleus. FOXO1 suppression in the adipocytes of steatotic patients may lead to the inhibition of the adiponectin receptors, blunting the autocrine action of adiponectin. Adiponectin operates as a key regulator of adiposity secretory function and prevents the release of several insulin resistance-inducing factors. Therefore, FKHR-dependent decimation of adiponectin may contribute to the induction and evolution of insulin resistance in the liver and skeletal muscle and stimulate accumulation of the lipids in the liver.

37. In summary, this in-depth study of WAT in NAFLD patients uses a systems biology approach to examine the molecular differences between progressive versus nonprogressive forms of NAFLD. WAT phosphoproteomic profiling points to an alteration in insulin signaling in the adipose tissue of patients with NASH versus SS, and supports the hypothesis that WAT is an endocrine organ that actively participates in the pathogenesis of NAFLD. These findings support the hypothesis that adipose tissue is an active participant in liver diseases that arise from metabolic alterations characteristic of obesity.

Analysis of Protein Signaling Networks in Metastatic Breast Cancer

38. We applied the LCM and reverse phase array technology as described in the '799 application to evaluate protein signaling networks in metastatic breast cancer. This analysis provides a new way to classify cancer based on functional signaling portraits.

39. *Molecular Classification of Human Breast Cancer Based on Functional Pathway Activation Portraits.* An underpinning hypothesis is that human breast cancer, despite the known heterogeneity of the disease, can be placed into common groupings based on commonly shared phosphorylation-driven signaling networks. To test this hypothesis, reverse phase protein microarray (RPPA) analysis of 25 human breast cancer surgical specimens was performed using 90 different phosphospecific antibodies. To begin to explore the potential for such functional grouping, we generated a broad-scale signaling

activation map to determine which signaling pathways are activated across a variety of human ductal carcinoma specimens, and if pathway-based clustering was apparent. As shown in Appendix 9, while patient-specific signaling is certainly apparent, there appears to be clustering of patients into subgroups broadly based on EGFR family signaling, AKT/mTOR pathway activation, c-kit/abl growth factor signaling, and ERK pathway activation. Moreover, it appears that some patients have tumors with overarching signaling activation across a number of pathways, while the rest of the patients' signaling portraits seem associated with specific pathway activation groupings. This result indicates that phosphorylation and cell signaling profiles are useful for the classification of breast cancer (perhaps as an example of other cancers) into functional direct groupings.

40. *Signal Transduction Analysis of Human Breast Cancer within the Metastatic Microenvironment.* To begin to determine the extent of the impact on ongoing cellular signaling within the metastatic lesion itself, we used RPPA technology (as described in the '799 application) to analyze the metastatic specimens from 11 patients with recurrent breast cancer that had metastasized to the liver following chemotherapy and compared the signaling fingerprints to the metastatic hepatic lesions from 18 other patients who had a variety of other primary solid tumor diagnoses, including pancreas, gallbladder, stomach, and melanoma cancers.

41. As shown in Appendix 10, a number of specific signaling activation events appeared to be specific to the breast cancer lineage, such as ErbB2 signaling, while other signaling molecules such as PKCR were much higher in the liver metastasis from other primary tumors compared to hepatic metastasis from breast carcinoma. These results indicate that a large number of cell signaling proteins are not differentially activated in the liver metastatic lesion regardless of the primary tumor type, which indicates that the hepatic microenvironment may provide a common milieu that provides a survival advantage for micrometastasis harboring specific signaling activation pathways regardless of tumor origin. However, there is a significant number of proteins whose phosphorylation state is statistically significantly altered based on tumor lineage. Activation and increased phosphorylation of ErbB2, for example, appear to be more prevalent in breast tumor

metastasis compared to other tumors analyzed. This does not mean that other tumors cannot be driven by HER2/neu signaling (which we know is possible) or that other types of metastasis may have high levels of receptor activation, but that this specific activation may be very important for the establishment of breast metastasis. Thus, these data provide direct evidence that the ongoing cellular signaling within the metastatic lesion may be unique and driven by both the "seed" (the organ where the tumor cell originated) and the "soil" (the microenvironment milieu of the metastatic site). The metastatic microenvironment seems to play a major role in determining the functional activation states of ongoing cell signaling in these study sets evaluated.

42. *Molecular Network Analysis of Signaling Pathways in Metastatic Breast Cancer from Patients Treated with Erlotinib.* While the search for biomarkers for early disease detection continues, and while the impact of routine mammography on earlier detection of breast cancer is clearly being recognized, breast cancer still is often detected in a metastatic setting. Development and clinical use of proteomic technologies and signal pathway profiling efforts in this setting will have to be performed under the auspices of microscopic quantities of input material from tiny needle biopsy specimens and fine needle aspiration. The experimentalist will not have the luxury of millions of cells grown in cell culture, but rather only a few thousand cells per input sample. RPPA technology provides a solution to meet this challenge. To demonstrate the practical utility of RPPA-based signal pathway activation profiling in a real-world clinical trial setting with a targeted inhibitor, we performed analysis of metastatic breast cancer cells from core needle biopsy specimens from a clinical trial that explored the therapeutic utility of Erlotinib.

43. Erlotinib (OSI-774, Tarceva) is a Human Epidermal Growth Factor Receptor type 1/Epidermal Growth Factor Receptor (HER1/EGFR) tyrosine kinase inhibitor. The target molecule of erlotinib, the EGF receptor, is overexpressed in 14–91% of breast cancers; the phosphorylation status of the EGFR and the overexpression of the receptor molecule itself are considered predictors for poor prognosis and reduced response rates to hormonal therapies. Erlotinib is thought to limit tumor cells' ability to divide, and may help to initiate apoptosis by preventing EGFR autophosphorylation and inhibiting downstream

signaling via MAP kinase and phosphatidylinositol 3-kinase/AKT pathways. However, little to no information is available concerning the actual effect of erlotinib on the EGF signaling pathway *in vivo* in human cancer cells.

44. In one study, we used reverse-phase protein array technology coupled with laser capture microdissection and phosphospecific antibodies to examine the activation status of several key signaling molecules in a series of 8 human breast cancer core biopsies taken before and after 1 month of oral Erlotinib administration. The aim of this study was to follow up on the published gene expression profiling analysis of the exact same tissue set and explore the feasibility of the RPPA platform to analyze small amounts of cellular material obtained by needle biopsy under conditions representative of what a targeted therapy trial would look like in a "real world" clinical setting. Moreover, we sought to test the hypothesis that the signaling networks of EGFR-mediated signaling would be altered as a consequence of the therapy, and could take advantage of the pre- and post-therapy patient-matched material in order to test the hypothesis.

45. Previously treated women with metastatic breast cancer (some had more than 3 prior regimes) were treated orally with 150 mg/d of Erlotinib and were biopsied at a chosen site of disease (liver, chest wall, skin, soft tissue, or lymph nodes) prior to treatment and 4 weeks after treatment. Epithelial cells from a total of 16 core biopsy samples (patient-matched pre- and post-erlotinib) were procured via LCM, and lysates from these samples were printed on nitrocellulose-coated arrays. Similar amounts of total protein across the test samples were demonstrated on the stained slides. The arrays were probed with phospho-specific antibodies against proteins representing 18 key points in a wide variety of signaling cascades with an emphasis on the phosphorylation levels of downstream end points of EGFR signaling pathways (e.g., ERK, AKT, STATs). Staining of the EGF-treated A431 cell lysate provided real time assessment of antibody and reagent performance.

46. The data indicated that the reverse-phase arrays are sensitive enough to detect extremely small levels of an analyte (2–10 ag/spot), and could be used for core needle biopsy samples that would be routinely employed in clinical trial tissue collection protocols. Compared to

EGF-treated and untreated A431 cell lysates as positive control, none of the patients evaluated in this study contained tumor epithelia with an overexpressed and/or hyperphosphorylated EGF receptor. This finding was consistent with IHC results as recently described for this study set.

47. Unsupervised hierarchical clustering analysis of the 22 EGF pathway-related phosphorylated and nonphosphorylated end points measured in this study (Appendix 11) revealed that the patient samples categorized into two generally distinct clusters, with the molecular network profile of 6/8 pretreatment biopsies falling into one cluster and 5/8 post-treatment portraits into another cluster. The unsupervised analysis indicated a general trend in that the chosen phosphorylated end points of interest appeared to be more highly expressed in the post-erlotinib group. Partition analysis of the data revealed that the normalized relative intensity values of pAKT (S473) and pEGFR (Y1148) were able to correctly segregate 14 out of 16 patients' samples as either pre- or post-treatment. Measurement of pAKT (S473) alone showed a statistically significant stronger staining in post-erlotinib treatment samples (p) 0.019) in each of the individual patient-matched specimens (Appendix 12A) as well as the entire post-treatment group (Appendix 12B). The phosphorylation and activation of AKT as a read-out for an apoptosis-inhibiting, pro-survival signaling pathway measurement may be, at first glance, contrary to the expected effect of the treatment with a tyrosine kinase inhibitor that is thought to increase the cell death rate in cancer. However, the array staining result is concordant with the clinical data of the trial, with progressive disease observed for all participating patients. Moreover, it is possible and perhaps predictable that a cellular response in the backdrop of a malignant process to an apoptosis-inducing agent would be to up-regulate the activity of a pro-survival pathway to mitigate and quell death-inducing signals.

48. Our results demonstrate the utility and feasibility of reverse phase protein microarray-based analysis for the multiplexed kinase substrate phosphorylation profiling from cells directly procured from biopsy specimens collected during targeted therapy trials. This exact study set had been analyzed previously for changes in gene expression patterns. In this pilot feasibility trial, 18 heavily pretreated patients with metastatic breast cancer were given

erlotinib and no clinical responses and no significant changes in tumor proliferation after erlotinib treatment were observed. While this study set did not include therapeutic responders, we chose to analyze the tissue from a subset of this group (8 patients, or 16 patient-matched pre and post specimens where tissue still remained for analysis) for phosphoprotein changes since patient-matched before and after therapy biopsies were still available.

49. Focused analysis of 22 key EGFR-related signaling end points revealed changes in cellular signaling events through treatment, disease progression, and between patients. The results continue to reinforce the results obtained earlier that indicate a large degree of patient-specific signaling and network heterogeneity. However, we observed a significant increase in pro-survival pathway activation within the post-treatment samples (Appendix 11) and Appendix 12). Unsupervised analysis of 22 protein end points, including 18 phospho-specific measurements, indicated a general partition of the pre- and post-treated specimens with the post-treatment group containing generally higher levels of phosphorylation, especially in the pro-survival pathway end points (Appendix 11). Statistical analysis reinforced this finding as pAKT levels were statistically significantly higher in the post-treatment set (p) 0.019). Interestingly, while none of these patients were classified as having overexpressed EGFR in the pretreatment cohort, the Y1148 phosphorylated isoform appeared to be slightly elevated in the post-treatment subset. These increases in phosphorylation of components of prosurvival signaling networks could be reflective of the clinical course of disease within these nonresponding patients and/or a result of adaptation of the cancer cells to escape apoptosis induction by the erlotinib therapy. This finding warrants further exploration in larger study sets.

50. Our results in this small study set of metastatic breast cancers revealed that the phosphorylation of the actual target protein for erlotinib, namely EGFR, was not significantly overexpressed in the patients' tumor cells. This result correlates with the

clinical outcome since none of the patients showed stable disease or remission during treatment. On the basis of this finding, in the investigated cases within our feasibility set, it is likely that activated molecular networks other than EGFR activation/phosphorylation may drive aberrant cell growth and tumorigenesis.

Analysis of Protein Signaling Networks in Wet Age-Related Macular Degeneration

51. Activity states for a plurality of different signaling proteins were measured in patients suffering from wet age-related macular degeneration using the methods described in the '799 application. The activity states for a plurality of different signaling proteins were studied in the vitreous fluid from individual patients suffering from wet age-related macular degeneration with the goal of identifying candidate therapeutic targets. We identified signaling proteins related to neovascularization, apoptosis, oxidative stress, adhesion, glucose/insulin metabolism and inflammation. In particular, significant differences in the activity states of different signaling pathways were observed among patients with wet age-related macular degeneration (Appendix 13). These data provide new therapeutic targets for a disease that has been refractory to treatment.

Conclusion

52. I further declare that all statements made herein of my own knowledge are true, and that all statements made on information and belief are believed to be true, and further that these statements were made with the knowledge that willful false statements and the like so made are punishable by fine and imprisonment, or both, under Section 1001 of Title 18 of the United States Code, and such willful false statements may jeopardize the validity of the application or any patent issuing thereon.

Respectfully,

Date July 28, 2008

By _____

Lance A. Liotta

APPENDIX 1.

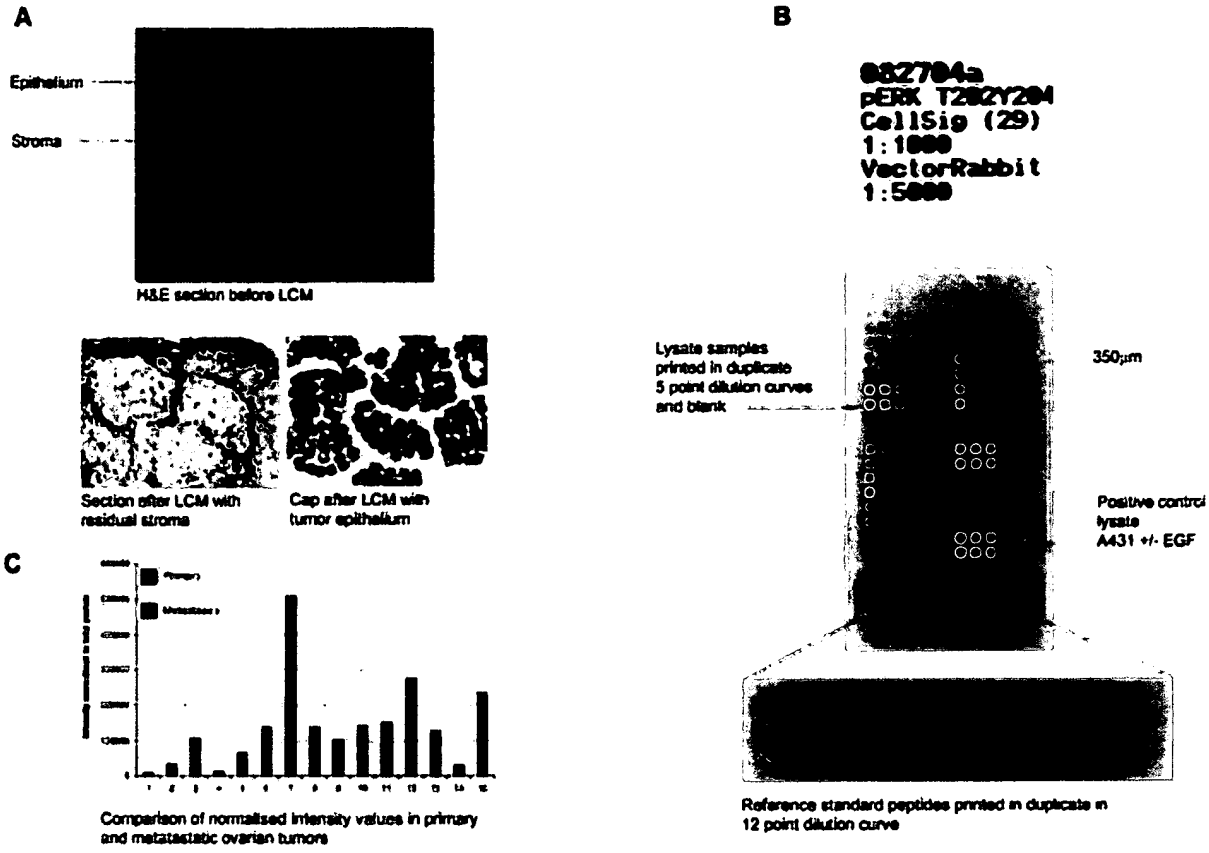

Application of reverse phase arrays in mapping molecular networks of ovarian cancer. A, using laser capture microdissection (LCM), ovarian cancer epithelial cells were isolated under direct microscopic vision from stained tissue sections leaving residual stroma on the slide. Approximately 25,000 cells were dissected for each case and lysed directly on the laser capture microdissection cap with extraction buffer. One hundred arrays were printed on nitrocellulose-coated slides. H&E, hematoxylin and eosin. B, example of an ovarian cancer reverse phase array probed for active extracellular signal-regulated kinase (ERK) signaling using a phosphospecific antibody detected with a tyramide-based avidin/biotin amplification system. Samples are printed in two columns: the left column represents primary tumors, and the right column represents metastatic lesions. Cases are printed in duplicate, five-point dilution curves to ensure the linear detection range for the antibody concentration is achieved. The sixth point represents a negative control consisting of extraction buffer alone. A positive control lysate (A431 squamous carcinoma cell line) is printed on the array for monitoring immunostaining performance. Phosphorylation-specific reference peptides are printed in a 12-point dilution curve on the bottom of the array for comparative, precise quantification of patient samples between arrays. pERK, phosphorylated extracellular signal-regulated kinase; EGF, epidermal growth factor. C, stained slides for the multiple phosphorylation-specific end points were scanned using Adobe Photoshop. Following total protein estimation with a Sypro Ruby stain, the intensity values of each antibody were normalized to total protein, and dilution curves were generated using Microvigene software. Histograms could then be generated to compare alterations in cell signaling between the primary and metastatic samples.

APPENDIX 2.

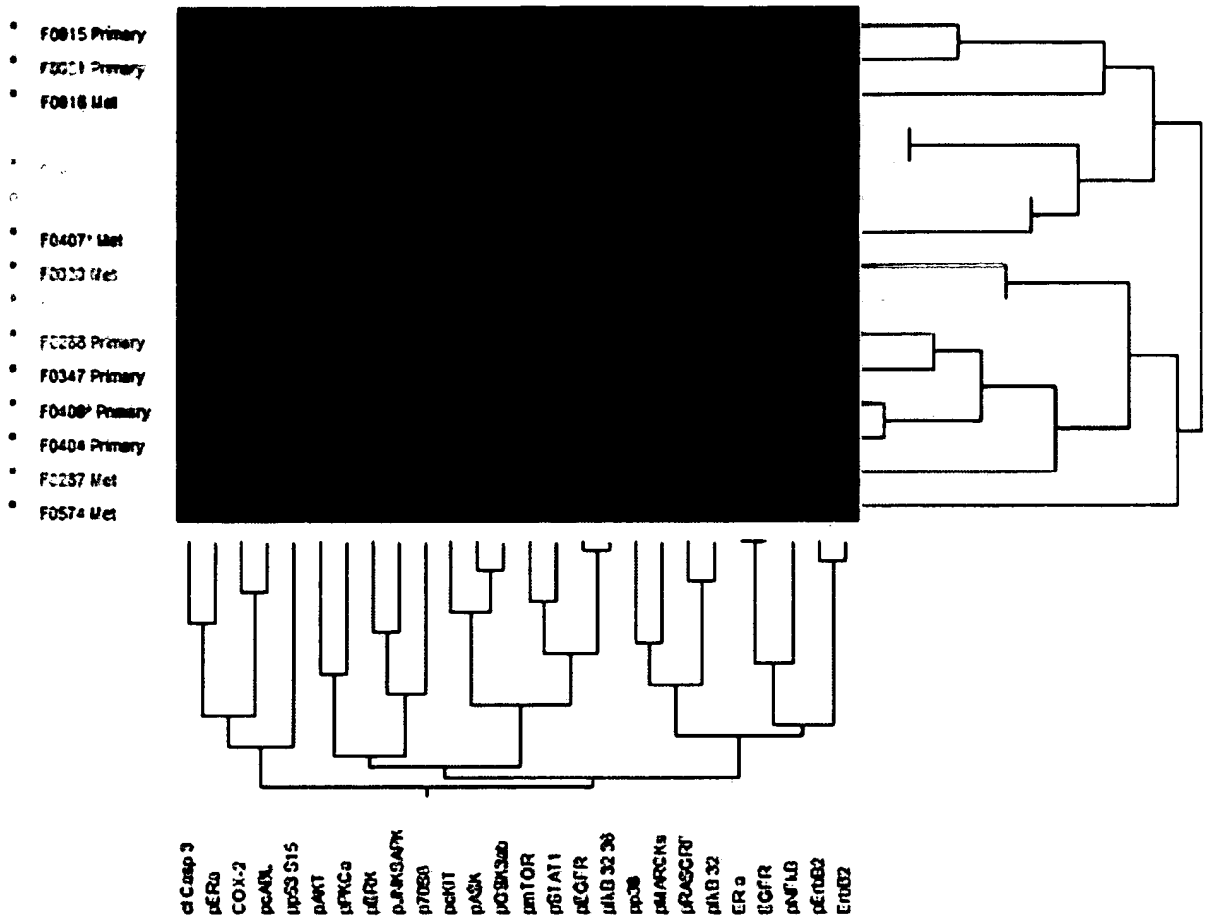

Unsupervised hierarchical clustering analysis of multiplexed kinase substrate end points. The multiple different kinase substrates are outlined on the horizontal axis, and the tissue phenotype is on the vertical axis. Higher relative levels of a phosphorylated substrate are represented in red; lower levels are in green. Matched cases are labeled in the same color type on the vertical axis, and unmatched cases are represented in black type. Met, metastatic tissue; cl Casp 3, cleaved Caspase 3; p, phosphorylated; ERα, estrogen receptor α; COX-2, cyclooxygenase-2; PKC, protein kinase C; JNK, c-Jun N-terminal kinase; SAPK, stress-activated protein kinase; GSK3, glycogen synthase kinase-3; mTOR, mammalian target of rapamycin; STAT, signal transducers and activators of transcription; EGFR, epidermal growth factor receptor; MARCKS, myristoylated alanine-rich C kinase substrate; ERK, extracellular signal-regulated kinase.

APPENDIX 3.

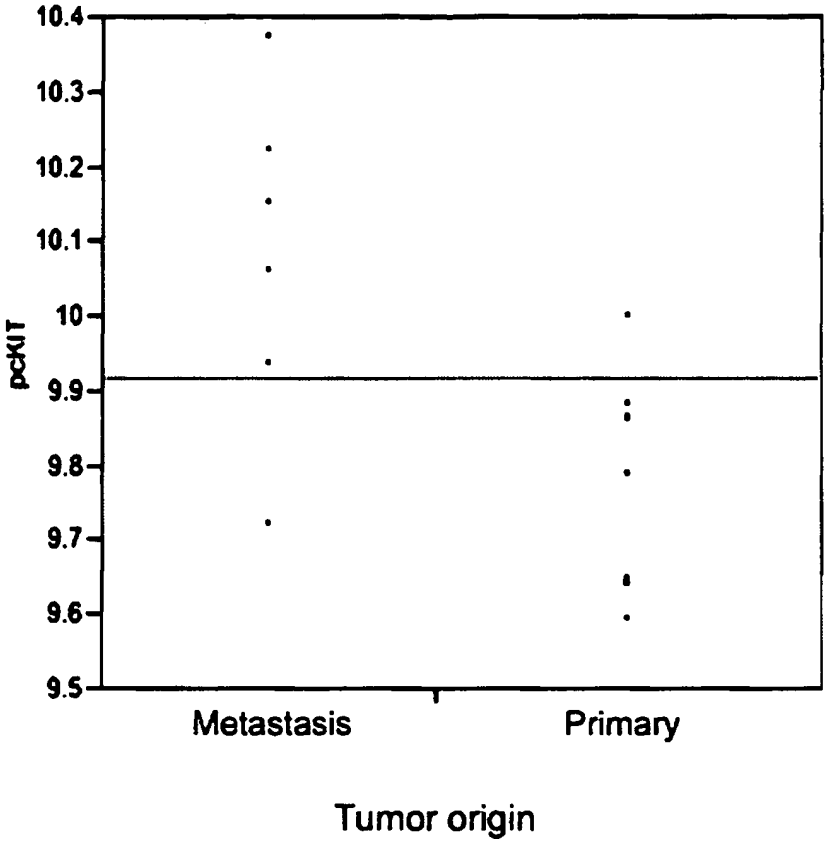

Analysis of phosphorylated c-Kit by tissue origin. Shown is the one-way analysis of normalized relative intensity values for phospho-c-Kit (pcKIT) demonstrating segregation of primary and metastatic tissue origins by this end point.

APPENDIX 4.

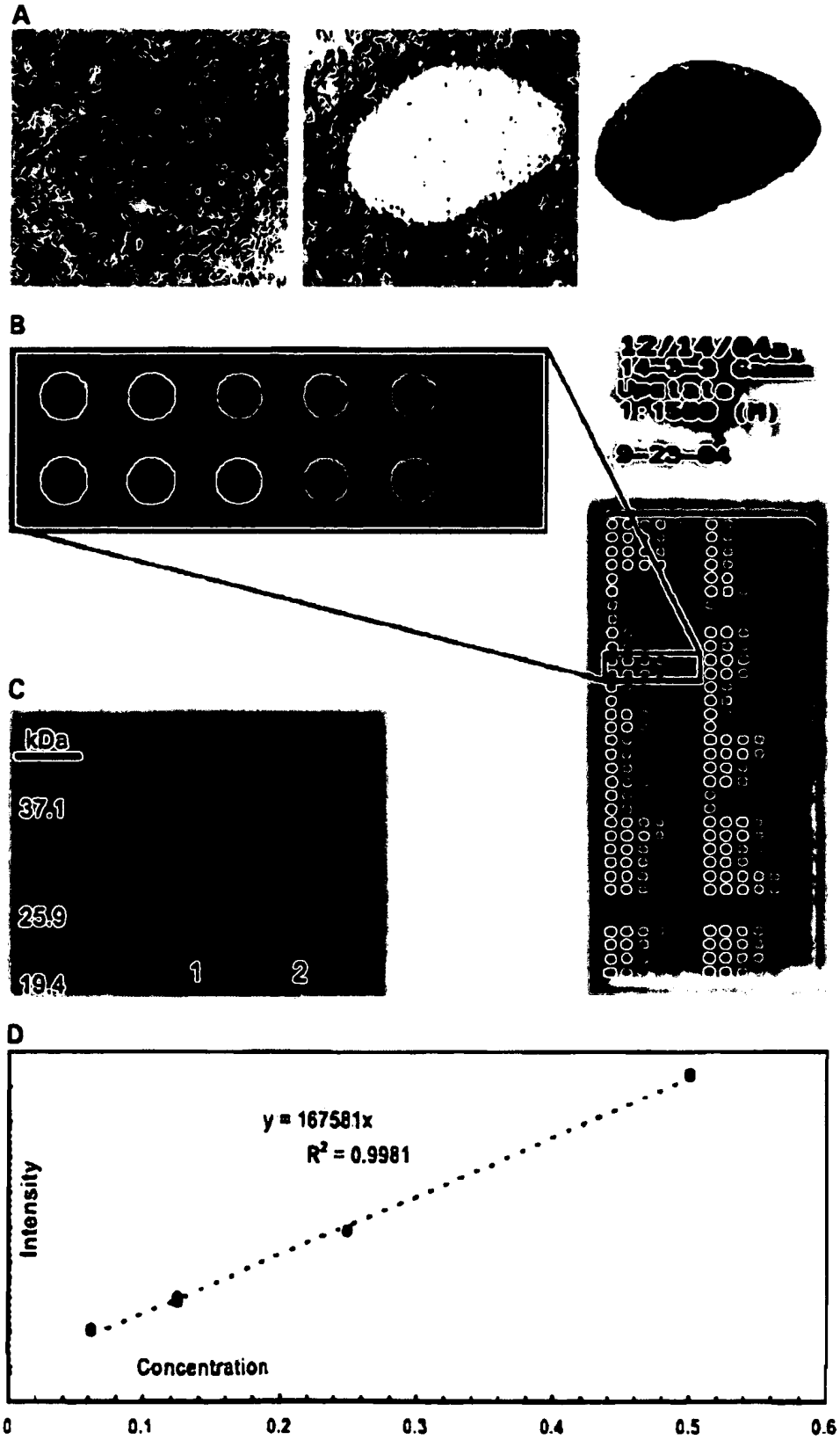
A
B
C
kDa
37.1
25.9
19.4
1
2
D
y = 167581x
R² = 0.9981
Intensity
Concentration
0
0.1
0.2
0.3
0.4
0.5
0.6

Schema for generating microarray data. A, lymphoid follicles were procured using laser capture microdissection (from left to right: hematoxylin-stained lymphoid follicle, tissue remaining after removing microdissected follicle, and microdissected follicle on polymer-coated cap). B, protein lysates from microdissected follicles were printed using a robotic arrayer in duplicate dilution series (neat, 1:2, 1:4,1:8, 1:16, lysis buffer control). Arrays then were probed with specific antibodies; in this case, for14-3-3g. C, each antibody was validated by Western blot. The protein shown is 14-3-3g (30 kDa): lane1, A431cell lysate; lane 2, follicular lymphoma lysate. D, arrays were scanned and mean pixel intensity was plotted against lysate concentration. Relative protein expression was calculated using the regression equation corresponding to the linear portion of the dilution curve.

APPENDIX 5.

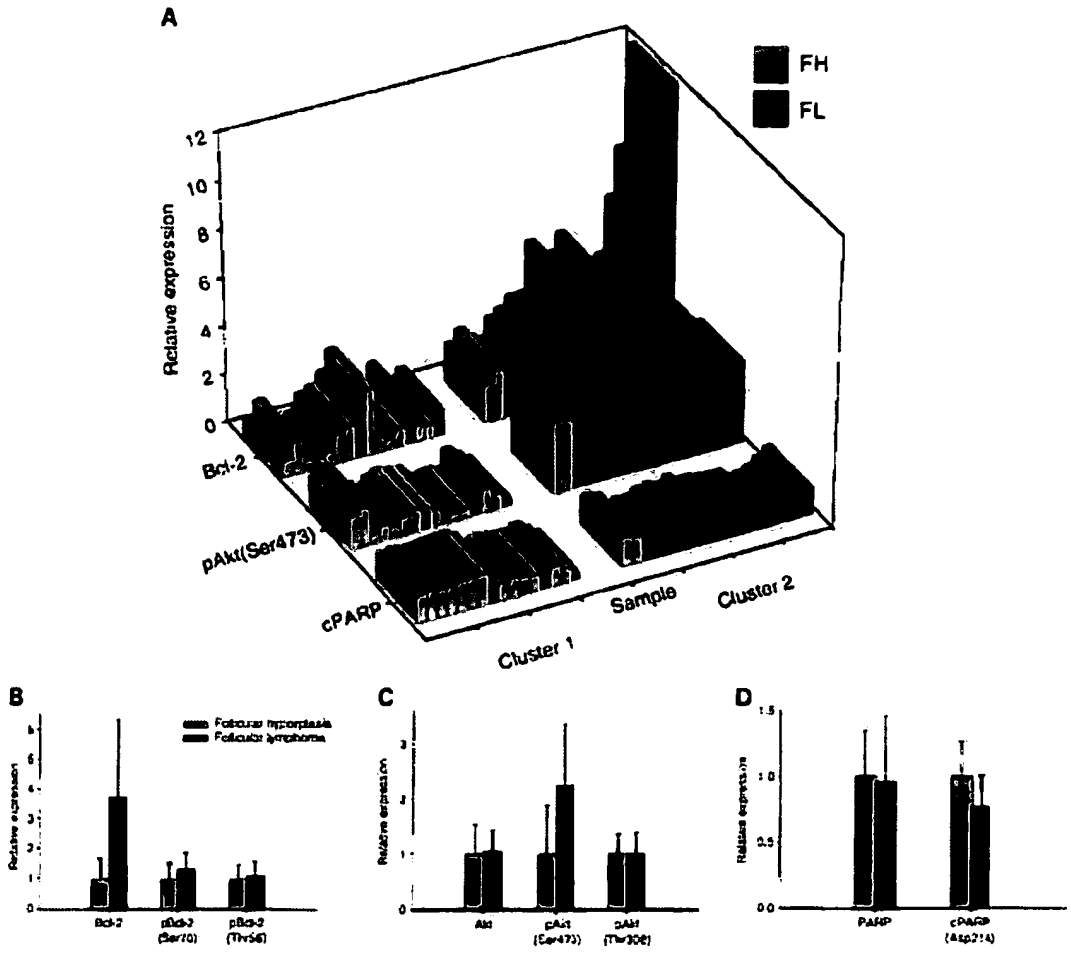

Principal component analysis of follicular lymphoma and follicular hyperplasia. A, based on the results of principal component analysis, hierarchical clustering was done using expression values for Bcl-2, phospho-Akt(Ser^{473}), and cleaved poly(ADP-ribose) polymerase (cPARP). Cases were segregated into two groups, one consisting of 13 FH cases and 3 FL cases (cluster1), and the other consisting of 17 FL cases and 2 FH cases (cluster 2). B, total Bcl-2, but not phosphorylated Bcl-2,was overexpressed in FL (black bars) compared with FH (gray bars ; $P < 0.0001$).Values are shown standardized to a mean FH value of1.0. C, phospho-Akt(Ser473)was overexpressed in FL ($P = 0.001$), but expression of total Akt and phospho-Akt (Thr308) was similar to FH. D, there was a trend toward lower cleaved poly(ADP-ribose) polymerase in FL cases ($P = 0.023$).

APPENDIX 6.

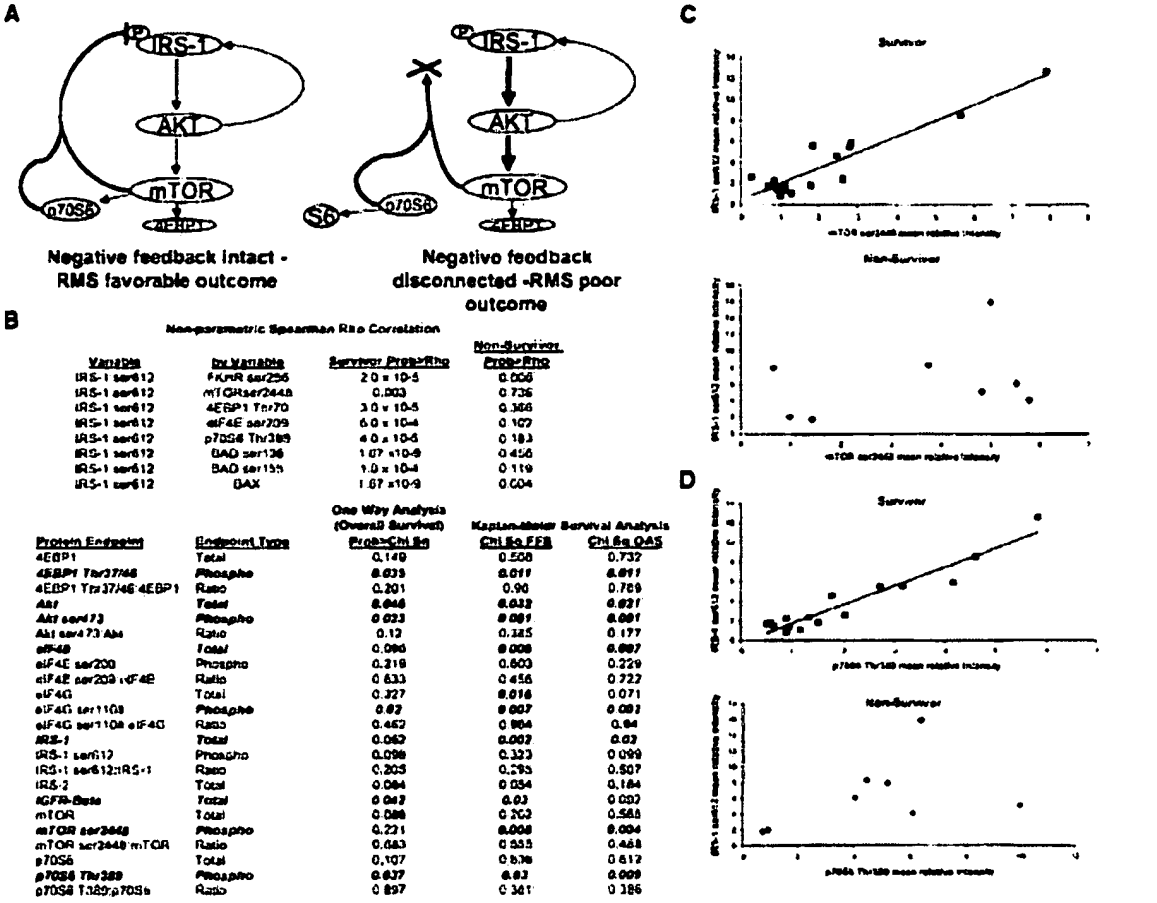

Proposed IRS-1 cell signaling pathway linkages in rhabdomyosarcoma study set 1B. A, IRS-1 feedback loop diagram. IRS-1 is regulated by both a positive feedback loop through Akt and a negative feedback loop through mTOR and p70S6 via IRS-1 Ser612. B, nonparametric and survival analysis of IRS-1/Akt/mTOR pathway proteins in sample set 1B. Spearman's Rho table of selected prosurvival and apoptotic signaling proteins evaluated for sample set 1B supports the hypothesis of an altered negative feedback loop between IRS-1 Ser612 and the Akt/mTOR pathway in patients with poor survival outcome. Comparisons are made between the total and phosphorylated form of the indicated end points. The phosphorylated form reaches a level of statistical significance ($P < 0.05$) compared with the total form of the protein, or the ratio of the phosphorylated to total protein. (Wilcoxon one-way analysis of overall survival outcome and Kaplan Meier log-rank survival analysis). C, Spearman's Rho nonparametric analysis showed a correlation between IRS-1 Ser612 and mTOR Ser2448 for tumors from patients with survivor status ($P = 0.0027$) compared with tumors from patients with nonsurvivor status ($P = 0.7358$). D, similar correlations were noted between IRS-1 Ser612 and p70S6 Thr389 for tumor samples from patients with survivor status ($P = 0.00004$) versus tumor samples from patients with nonsurvivor status ($P = 0.1827$).

APPENDIX 7.

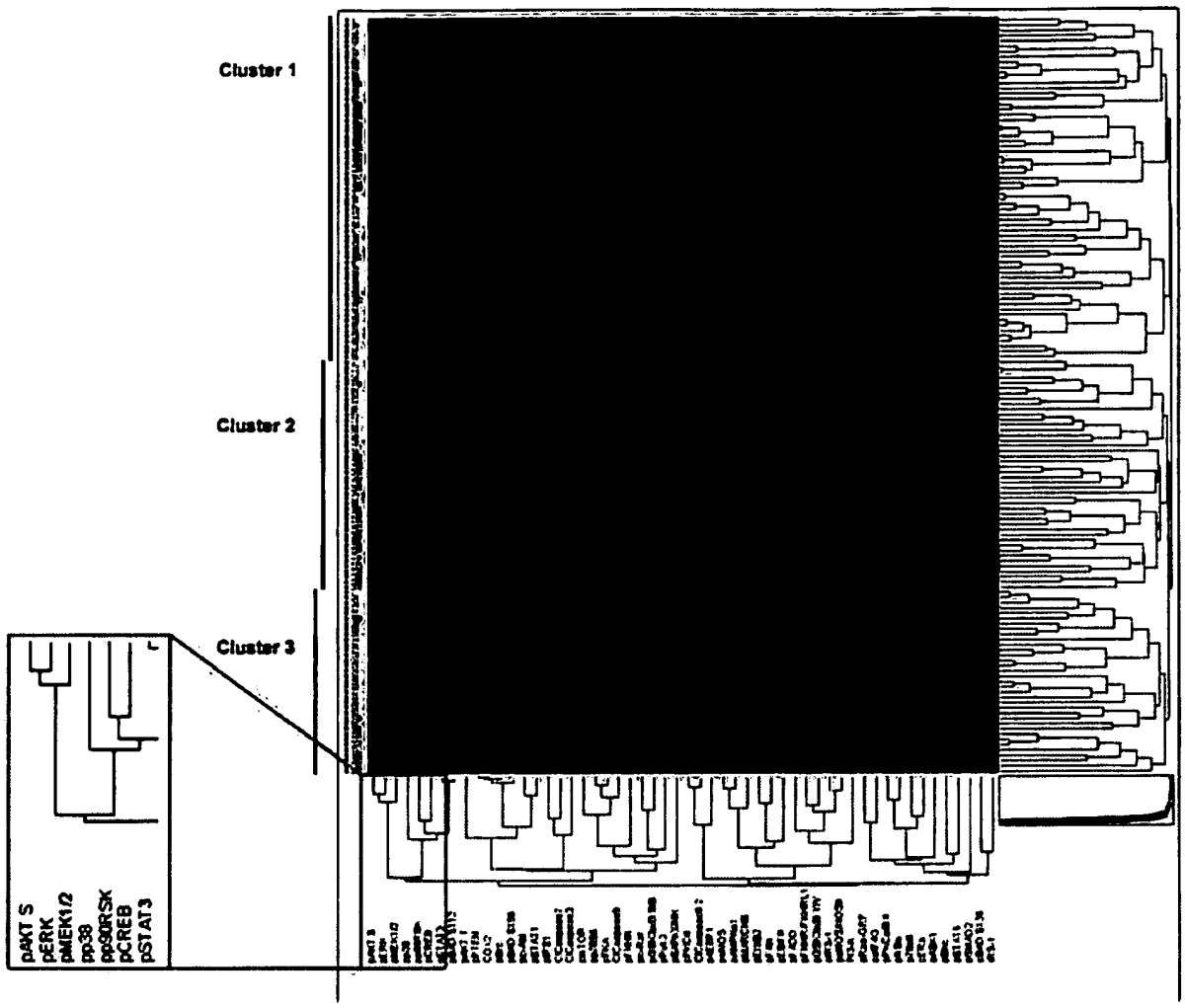

Unsupervised molecular network analysis of cell signaling pathways. Bayesian two-way clustering of endpoints (X-axis) and patients (Y-axis) is shown as a heatmap where degree of relative levels of phosphorylation are shown, with red indicating the highest relative level of phosphorylation within the study set, green the lowest relative level, and black indicating the median relative level. Three major clusters were formed, none of which correspond to liver disease pathology, and generally differed by degree of broad pathway activation. Cluster 1 contained patients with generally indolent adipocyte signaling, cluster 2 contained patients with generally broad signaling activation, and cluster 3 with a mixed phenotype. The ability of the RPA and clustering to faithfully recapitulate ongoing kinase driven signaling is demonstrated in the magnified box at the left, where the MEK-ERK pathway segregated into a unique family set. This clustering occurred without *a priori* training.

APPENDIX 8.

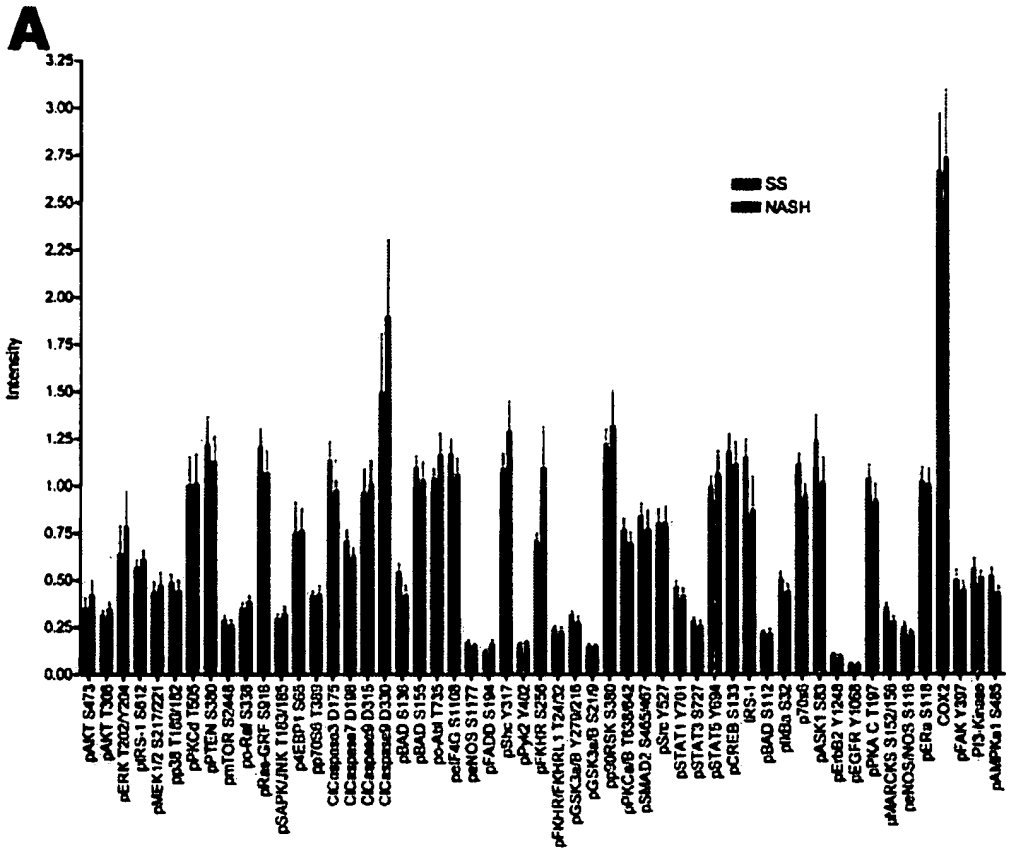
A
Intensity
SS
NASH
pAKT S473
pAKT T308
pERK T202/Y204
pIRS-1 S612
pMEK1/2 S217/221
pp38 T180/182
pPKCd T505
pPTEN S380
pmTOR S2448
pc-Raf S338
pRas-GRF S916
pSAPK/JNK T183/185
p4EBP1 S65
pp70S6 T389
ClCaspase3 D175
ClCaspase7 D198
ClCaspase8 D315
ClCaspase9 D330
pBAD S136
pBAD S155
pc-Abl T735
pcIF4G S1108
peNOS S1177
pFADD S194
pShc Y317
pPyK2 Y402
pFKHR S256
pFKHR/FKHRL1 T24/32
pGSK3a/B S21/9
pGSK3a/B Y279/216
pp90RSK S380
pPKCa/B T638/642
pSMAD2 S465/467
pSrc Y527
pSTAT1 Y701
pSTAT3 S727
pSTAT5 Y694
pCREB S133
IRS-1
pBAD S112
pRBs S32
p70s6
pASK1 S83
pErbB2 Y1248
pEGFR Y1068
pPKA C T197
pMARCKS S152/156
peNOS/NOS S116
pERs S118
COX2
pFAK Y397
PI3-Kinase
pAMPKa1 S485
B

Analysis of specific signaling endpoints in adipose tissue taken from patients with progressive versus non-progressive NAFLD. (A) This histogram shows relative levels of phosphorylation of each of the signaling endpoints. Statistical significant differences (P"0.001) between NASH and SS with or without NSI was seen with phosphorylation of FKHR (denoted by asterisk). (B) Principal component decision tree of the same subjects reveals only components of the insulin signaling axis as important discriminators.

APPENDIX 9.

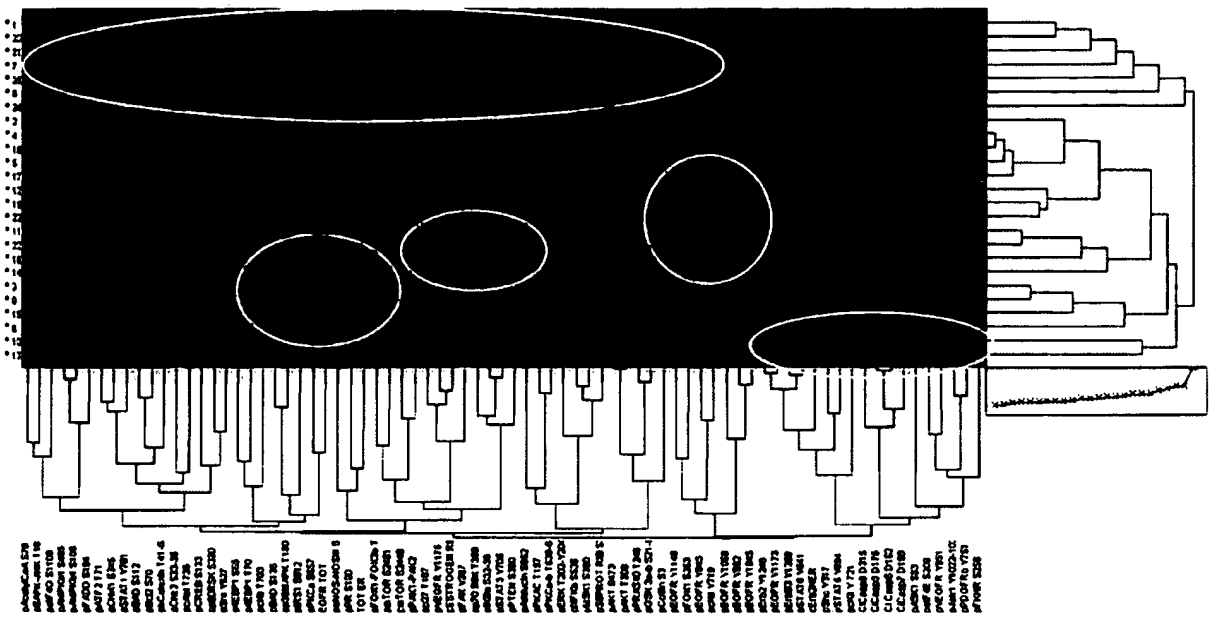

Unsupervised hierarchical clustering of breast cancer surgical specimens. Patient samples are oriented on the vertical axis and the signaling end points tested are oriented on the horizontal axis. Clustering of patients into subgroups broadly based on EGFRfamily signaling, AKT/mTOR pathway activation, c-kit/abl growth factor signaling, and ERK pathway activation is apparent.

APPENDIX 10.

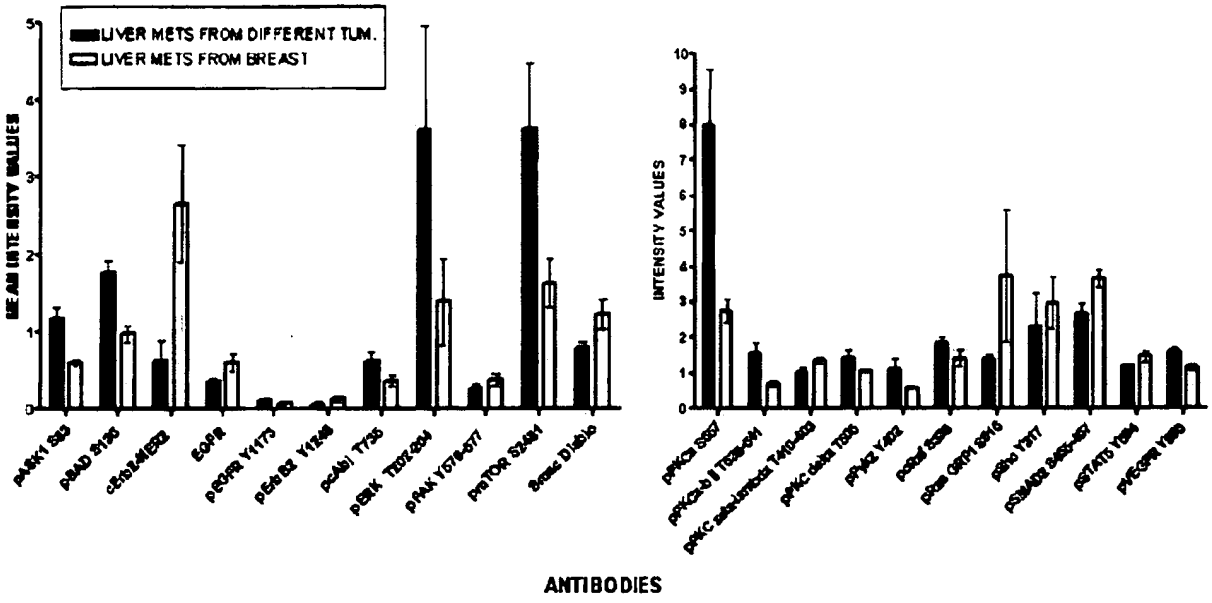

Comparisons of the average normalized intensity values for signaling end points statistically different between liver metastases from breast cancer and liver metastases from other various primary tumors. Error bars refer to SD from the mean.

APPENDIX 11.

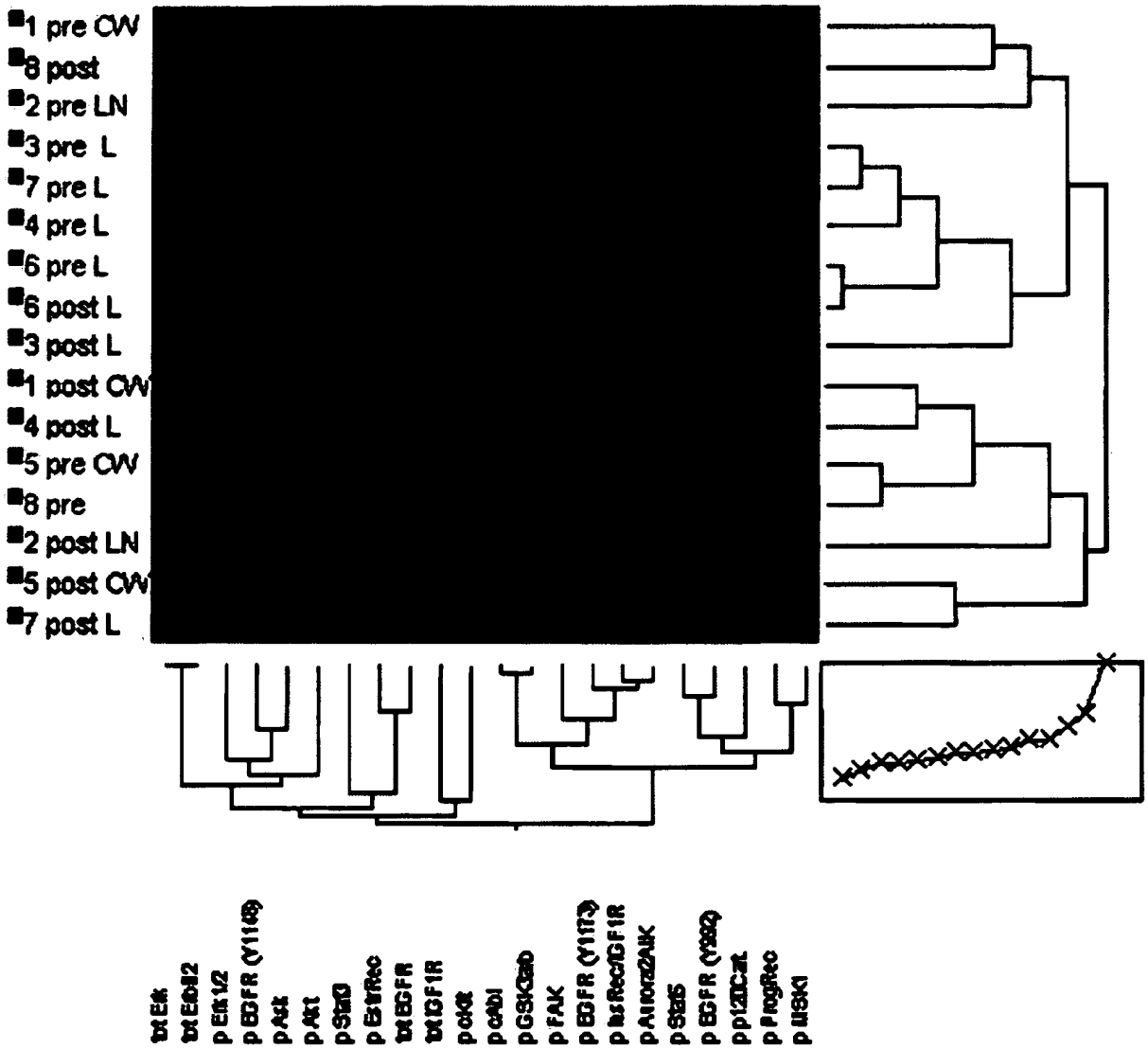

Unsupervised hierarchical clustering analysis of multiplexed kinase substrate end points. The multiple different kinase substrates are outlined on the horizontal axis, and the pre- and post-treatment samples are on the vertical axis. Higher relative levels of a given analyte are represented in red; lower levels are in green. Matched cases are labeled with the same number on the vertical axis.

APPENDIX 12.

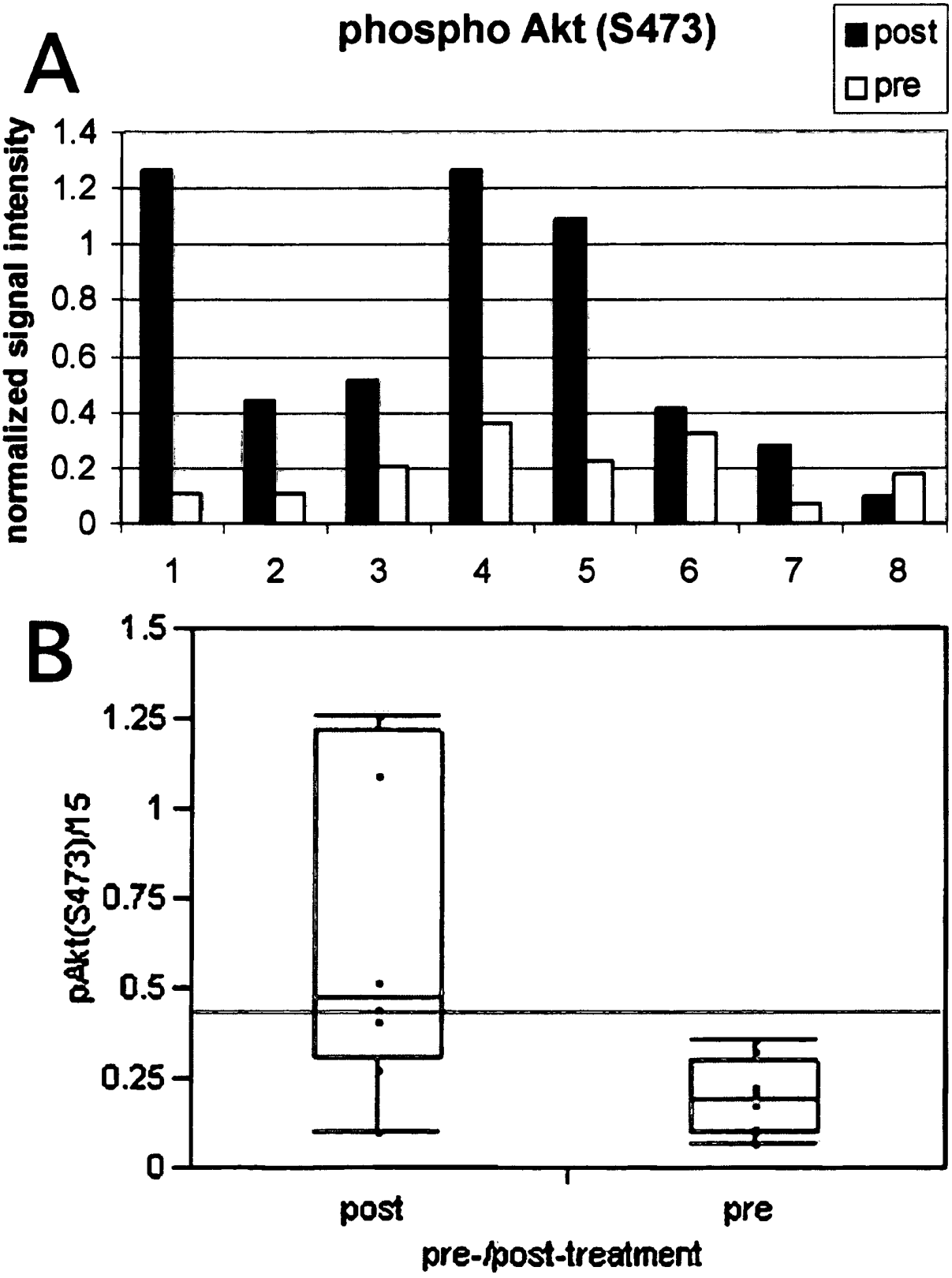
A
phospho Akt (S473)
post
pre
normalized signal intensity
1.4
1.2
1
0.8
0.6
0.4
0.2
0
1
2
3
4
5
6
7
8
B
1.5
1.25
1
0.75
0.5
0.25
0
pAkt(S473)/15
post
pre
pre-/post-treatment

Comparisons of phospho AKT (S473) levels in metastatic breast cancer before and after erlotinib treatment: Statistically significant increased signaling for pAKT (S473) in posttreatment samples. Normalized intensity values were averaged among each separate patient matched samples (A) and among the pre- and post-treatment tumor specimen group (B). Error bar) SD from the mean.

APPENDIX 13.

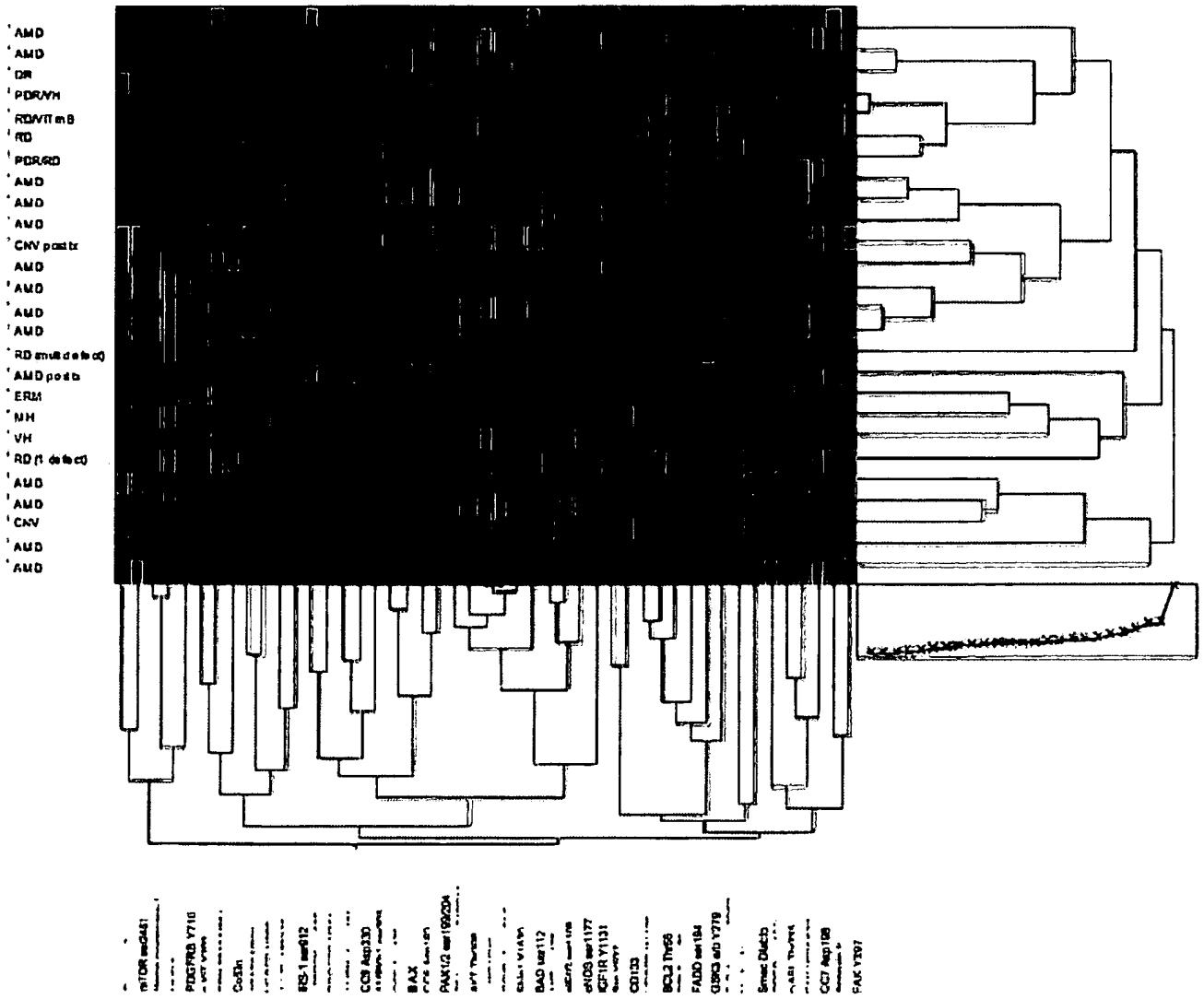
AMD
AMD
DR
PDR/VH
RD/VH in B
RD
PDR/RD
AMD
AMD
AMD
CNV post tx
AMD
AMD
AMD
AMD
RD (multi defect)
AMD post tx
ERM
MH
VH
RD (1 defect)
AMD
AMD
CNV
AMD
AMD